VOL. 7, NO. 6, JUNE 2012 ISSN 1819-6608
ARPN Journal of Engineering and Applied Sciences


www.arpnjournals.com

AN INEXPENSIVE SHIELDED ACOUSTIC PROBE FOR PRESSURE MEASUREMENTS NEAR A RADIATING ULTRASONIC TRANSDUCER

Peter W. Higgins and Corinne S. Lengsfeld
Department of Mechanical and Materials Engineering, University of Denver, S. York St., Denver, Colorado, USA
E-Mail: peter.higgins@du.edu

ABSTRACT

There is a need to detect the details of acoustic pressure fields in experiments near ultrasonic radiators being driven by high voltage signals which broadcast electromagnetic radiation, EMR, into the measurement media. Ultrasonic fields are being generated in fluids for the manufacture of unique materials through sonochemistry, and there is new interest in the degradation of biological molecules from such fields. Conventional field measuring sensors such as hydrophones, thermistors, and thermocouples are susceptible to contamination by the voltage signal emanating from the ultrasonic field generator when there is any contact with the measurement medium. Such EMR, entering the zone of measurement can be orders of magnitude greater than the voltage resulting from the measurement of the field itself. This work describes the design and characterization of a piezoelectric (PZT) planar disk encased within a separately grounded Faraday cage to act as a pressure field sensor. It is demonstrated that the separate grounding of this cage effectively eliminates the EMR contamination. Further, the work describes a calibration procedure incorporating a force beam to translate strain from a static load, and then from a dynamic load at the frequency of interest. Experimental measurements with this probe design show a near 80% correlation to a theoretically calculated wave form using ray tracing to simulate the pressure field in the test cell.

Keywords: ultrasonic field sensor, Faraday cage shielded ultrasonic probe, pressure measurement.

INTRODUCTION

There is a growing body of literature that documents the degradation of biological molecules from ultrasonic pressure waves [1, 2, 3, 4, 5]. For example, Wu [1] concludes that 'cavitation is considered as a primary mechanism for the ionization of biomolecules.' He cites cavitation bubble collapse energy release as promoting chemical reactions and ionizations such as reported for polymerization of benzene and CO_2. But, little is understood about how to control or mitigate degradation because of a lack of detailed fluid dynamic characterization of the system. Additionally, the use of ultrasonics to carry out unique chemistry for material fabrication is of current interest [6], [7]. Gedanken [6] describes sonochemistry as one of the first techniques used to prepare nanosized compounds. He mentions, for instance, insonating Fe $(CO)_5$ to get iron nanoparticles. Both research areas would benefit from a detailed understanding of the pressure field within the fluid system. Under these operating conditions measurements are necessary close to an ultrasonic source in contact with the liquid media. When close to an ultrasonic transducer driven by high voltage, probe designs are susceptible to electromagnetic interference (EMI) from EMR because the sensor connections act as an antenna. There is, therefore, a need for a small acoustic field pressure probe that can resolve the temporal and spatial fluctuation of the field when submersed close to a radiating piezoelectric source. This work documents the design and calibration of such a probe, and then evaluates its performance relative to theoretical predictions within a system that contains both a primary wave and reflections.

Commercial hydrophones are intended for pressure field measurements distant from sources of acoustic radiation. However, when operated close to a high voltage source, the primary electromagnetic radiation (EMR) emanating from the source needs to be subtracted, if known, or filtered [8] to isolate the voltage signal resulting from the hydrophone's sensor. Prior knowledge of the phase delay and amplitude of the EMI at that location is required. Uncertainties in these assumptions will impart error onto the actual pressure field signal, especially when the signals of interest are more than one order of magnitude lower than the driving voltage signal. Many hydrophones are also too large to work in small test cells. Commensurate with large size, such devices have unknown, or uncertain, acoustic centers to resolve to a point in space.

There are several novel approaches to modify hydrophone operation to address specific issues. For example, to resolve position specificity, others have used a PZT ultrasonic sensor attached to a 20 cm long tapered acoustic horn [10]. These long horns have the potential to amplify the EMI problems. Bushberg [11] demonstrates a metal cage partially surrounding the PZT element without grounding to help with measurement noise. Neither of these completely shields the PZT probe from EMI from the primary ultrasonic transducer source. Therefore, although appropriate for distant measurements, these devices will exhibit signal contamination close to a contacting source.

An alternative approach to measuring the pressure field has been to use thermocouples or thermistors [12], which are designed to make the active element (i.e., tip) an energy absorber. These devices

proved incapable of quantifying acoustic fields to the desired accuracy or repeatability (unpublished work). Pugin [13] also concludes that these devices provide only a rough approximation of local maxima and minima. Susceptibility to EMI is not discussed in any of these papers. Data taken in our lab shows the connecting lead wires of these systems act as effective antennas when placed close to the source.

Durkee [14] promotes the use of strips of aluminum foil to evaluate the field strength over a cross sectional area of an ultrasonic cleaning tank [13]. In principle, stronger pressure fields produce pitting of a thin aluminum foil after about 10 minutes exposure. This technique was tried following the recommended practice. It was found that pitting was not significant, and that neither test had any temporal resolution, and only the rigidly supported strip had spatial resolution. However, the technique is immune to EMI problems.

Witte [15] reaffirms the need for low cost acoustic field sensors and describes a disposable hydrophone. The device transforms acoustic pressure into electrical energy based on the Auger Effect, relying on conductive rather than piezoelectric materials as a sensor. The device described targets the higher frequencies used in medical applications with the lowest test conducted at 540 kHz. The devices' susceptibility to electromagnetic interference (EMI) is unknown.

Employment of a screen wire Faraday cage surrounding a PZT element sensor has been reported previously by Felizardo's group [9] during an attempt to detect the shock wave generated by bubble nucleation. In this case the sampling frequency was below 10 kHz. It was determined that the addition of a Faraday cage could induce noise into the preamplifier. A design that did not include preamplification within the probe assembly was not discussed. It is highly probable that lower frequency contamination observed could be eliminated with an alternate design.

OBJECTIVE

Since no simple inexpensive means of quantifying the acoustic field environment near the radiating source (within 10 cm) was found, the objective of this work was the design of an acoustic probe having an appropriately sized planar PZT disk within a grounded Faraday cage for quantitatively measuring the pressure waves emanating from a 44 kHz driven ultrasonic transducer submerged in water. A secondary objective was the development of an accurate calibration method which would enable quantitative temporal and spatial characterization of the pressure field. To assess whether both objectives were met the probe performance was compared to a simulated 44 kHz wave with reflections.

This paper presents the construction of a probe that can resolve the temporal and spatial fluctuation of an acoustic pressure field near a radiation source. The probes' operating characteristics and methods for calibration are outlined. Then three measures to validate the sensor output are discussed: (i) comparison of the unshielded and shielded signals for magnitude and composition; (ii) comparison of experimental measurements to results by ray tracing; (iii) direct measurement of phase patterns. Finally, results from experimental measurements at multiple locations are provided as evidence that spatial differences can be resolved.

DESIGN, FABRICATION AND CHARACTERISTICS OF SENSOR

Design

The probe assembly pictured in Figure-1 was constructed for approximately $50 USD. The round 15 mm diameter, 0.9 mm thick PZT sensor was purchased from Steiner and Martins, Inc. It is made from SM111 PZT4 material having resonant frequencies of (Thickness) 2.2 MHz ± 50 KHz and (Radial) 135 kHz ± 5 KHz. The resonant impedance, $Z_{m,}$ is (Thickness) ≤1.55 Ω (Radial) ≤11 Ω, while the static capacitance is 3481 pF±15 % @ 1 kHz. The sensor is installed vertically, aligned with gravity. The disk is bonded by flexible Silastic to an electrically insulated pin (instead of a backplate) located on the centerline of a separately grounded, stainless-steel Faraday cage (tea stick infuser, Item # 800790, available from REI). A backplate is not needed in this application because its first resonant frequency (135 kHz) is much higher than the range of its intended use (20-80 kHz) so no attenuation of its resonant Q is required. A front wear plate is also not needed since the sensor is protected by its Faraday cage, and long term, continuous use is not envisioned. No preamplifier is housed within the enclosure, because it is intended to be used within 2 m of a sensitive recording oscilloscope which serves as the preamplifier. Sensor connection wires are encased within a shielded instrument cable and mounted rigidly within the cage to reduce strain on the PZT disk. A separate ground wire for the Faraday cage is connected to the assembly, and is grounded at the recording oscilloscope ground. Probe signals are output in a shielded instrument cable terminated with a BNC electrical connector.

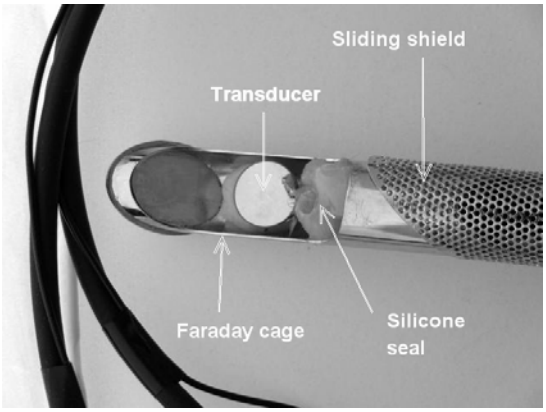

Figure-1. Image of sensor, sensor assembly and Faraday cage.

Selecting cost effective PZT elements requires some characterization to ensure performance can be achieved within experimental tolerances. For example, planar disks are known to respond differently depending on their orientation with respect to the source. Characterization of 15 mm PZT radiation directivity can be approximated [16] and is shown in Figure-2. For a baffled disk (assuming the Faraday cage approximates a rigid baffle), the far field spatial pressure variation directivity factor is given by equation 1:

$$p(\vec{r}) = \frac{2J_1(ka\sin\theta)}{ka\sin\theta} \quad (1)$$

where k is the wave number, a is the disk radius in meters, r is the vector to the far field point in meters, J_1 is the Bessel function of 1st kind, and θ is the angle from normal in radians.

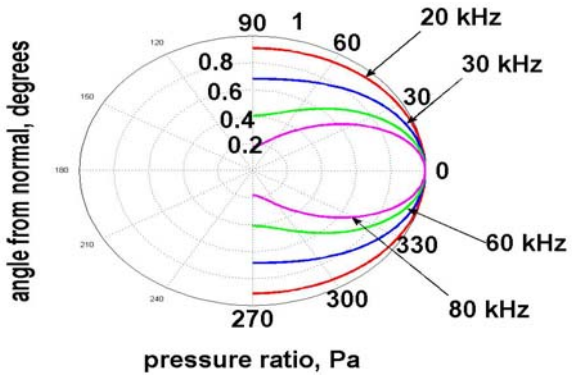

Figure-2. A polar plot of the normalized radiation reception pattern for the 15 mm PZT probe evaluated from 90 to 270 degrees for 20, 40, 60 and 80 kHz acoustic fields.

The results of the orientation dependency study, Figure-2, demonstrate that a broader (more uniform) response is obtained for the lower frequencies presented within this work. Moreover that precision alignment of the sensor and driving transducer face is also not required.

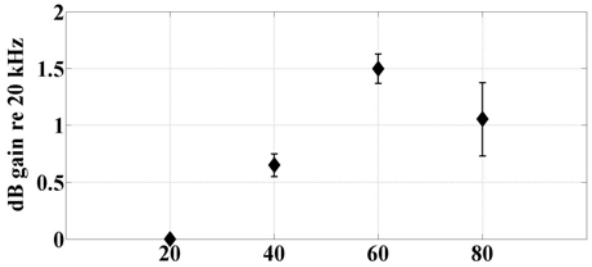

Figure-3. Probe signal response as a function of frequency (e.g., 20, 40, 60, and 80 kHz). Error bars represent a ± 0.2 E-05 volt uncertainty in the signal voltage reading which amounts to approximately 10%.

The frequency response of the probe is examined at the same four frequencies used to calculate angular response above to demonstrate that this PZT element will be excited by the intended driving transducer for determining the range of useful application. This is accomplished by measuring the voltage signal output of the probe along with the (RMS) power delivered to the radiating transducer at each frequency. The voltage squared output of the probe is adjusted to the same radiated power level, then the db response is computed as 10 log of the response relative to the response at 20 kHz. By convention, the sensitivity should be measured in an anechoic environment, but this is a difficult measurement to make because the reflective environment in the test tank, produced by pressure reflections from the walls of the test cell, produce nodes and antinodes near the probe which are functions of frequency as is modeled later in this paper. To overcome this effect the measurements made for the sensitivity study were pre-echoic. This means that the output of the probe was recorded by a high speed memory scope in single sweep mode to capture the probe response before being influenced by reflections. Considering the probe - radiating transducer distance was 7 cm, and the speed of sound in water at 20 C is 1481 m/s, the signal arrives at the probe in ~50 µs. But reflections from the nearest wall are at least 4 times this interval arriving after another ~200 µs. The measurements for Figure-3 were taken before 100 µs thus avoiding the influence of reflections. The dB variation of probe response over 20-80 kHz is given in Figure-3, showing a nearly flat response over the frequency range. This frequency response behavior is consistent with the findings of Lewin [17].

Sensor calibration

The transient and non-linear nature of the pressure field makes calibration of probes to measure the pressure magnitude difficult. The use of force measuring beams for calibration for other pressure sensors is not new, and has been reported by others [18],[19]. It was decided to use a force beam apparatus that could be submersed in the water so as to directly measure the dynamic load of the transmitted signal at any desired frequency. Based on our prediction of the driving transducer's pressure load, a beam sufficiently flexible to deform under gram loads is selected. The flexible beam is a 12 cm long, 1.3 cm wide, and 1 mm thick copper strip sheared from a plate. An Omega Engineering, Inc type KFG-3-120-C1-11L1M2R 120 Ω strain gauge is mounted 7 cm from the clamped end. A 15 mm PZT disk, identical to the probe's sensor, is attached to the tip of the flexible beam. It is important to create an identical target area, and to ensure that the strain gauge is not measuring the uncoupled vibration of a mass on its tip in addition to the acoustic field.

A Fluke model 8840A/AF precision digital desktop meter (accuracy = ± 1 mΩ) is used to quantify beam response to bending under a static (i.e., known mass) and dynamic (i.e., acoustic forcing) load. As constructed and under no load, the measured resistance is 122.389 Ω, while a 20 g static load produces a resistance reading of 122.411 Ω. Because the strain gauge is a thin foil, slight

temperature dependence is expected and observed, which is overcome by multiple readings. The resultant, experimentally determined, calibration curve slope for the force beam strain gauge under a static load is 22 mΩ/g.

The forced beam response is also observed under dynamic loading conditions. The beam is insonated by both a 44 kHz ultrasonic transducer that is driven at 20 W (electrical) and positioned 2.5 cm from the transducer face, and by an identical (to the sensor and to the target) 15 mm ultrasonic transducer at 45 kHz and at the same distance. For clarity the setup using the larger source is shown in Figure-4. The accompanying PZT element response is observed and directly correlated to the strain gauge output from the force beam in terms of V/Pa to complete the probe calibration. For both static and dynamic loads on the beam, direct measurement of the change in resistance of the gauge is done by allowing the gauge resistance to stabilize in time, offsetting the gauge to its rest value to read zero, and then quickly making the difference measurement. This accounts for temperature drift and additional resistance from wires and connections, which can change over time. The procedure is typically done six times and the results are averaged. Voltage measurements from the gauge are not useful because the gauge and its wiring have the same antenna effect as an unshielded probe. This method of reading the strain gauge probably resolves the criticism of strain gauge beams raised in reference 18.

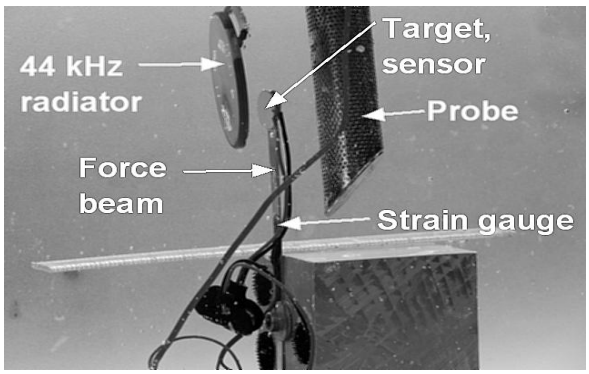

Figure-4. Photograph of force beam calibration device with grounded target being insonated by a secondary standard transducer.

PERFORMANCE VALIDATION

Experimental methods

Different test scenarios were experimentally explored to verify that (a) the probe design isolated the transducer voltage induced EMI sufficiently to use the measured signal without other filtering or isolation methods, and (b) the probe could measure the detailed pressure field produced by an ultrasonic source:

a) Insonation of a single probe located between two continuous sine wave radiating transducers, one at 24 kHz, the other at 30 kHz (Figure-5). The purpose is to study the probe resolution of a complex acoustic environment, and to verify a phase shift in the detected signal. The latter objective is accomplished by displacing one of the radiating transducers 3 cm farther from the other while keeping the first transducer and the probe fixed in place. The results of these measurements (Figure-6) are compared to an acoustic model of the expected field that accounts for the magnitude and phase contributions of chosen acoustic rays to the calculated field at the center of the probe sensor location. The chosen rays model direct radiation and 1st reflections from the top, bottom, sides and back glass surfaces. Multiple reflections are not considered.
b) Insonation of a single probe by a single transducer that is driven by a square wave to produce a complex field. The probe response is recorded with the Faraday cage grounded and ungrounded in order to quantify the degree of isolation from EMR when grounded (Figure-7). Discrete Fourier Transforms are calculated from samples of these signals to produce frequency spectra of the driving voltage signal, and of the transformed received signal from the grounded, and ungrounded probe, which helps establish that the grounded probe isolates the acoustic signal from induced EMR (Figure-8).
c) Two probes of this design are radiated by a continuous sine wave, then one is moved 2 cm with respect to the other to further study complexity resolution and associated phase change (Figures 9-10). Lissajous patterns are recorded to verify the detected phase change. These patterns are created by plotting on an oscilloscope the response of one probe on the ordinate and the other probe on the abscissa. The gain of the two channels is the same.

Experimental apparatus

A 20°C water-filled 8 L aquarium was used in the reported experiments to evaluate performance. The tank is glass-sided measuring 30 cm by 15 cm with a water height of 19.5 cm. The radiating transducers were 5 cm diameter by 0.3 cm thickness, PZT, SM111, planar mode vibration disks purchased from Steiner and Martins. These have a nominal natural frequency of 44 ±3 kHz and an impedance of < 8 Ω. Transducer driving signals were continuous sine waves in two experiments, and a square wave for the third. These were produced by a Leader, LAG 1208 Audio Signal Generator, and by a Victor VC 2002 digital frequency generator. Amplification of the driving signals was accomplished using a Crown Vs 1100, and a 240W dual channel amplifier, and recording was done with a Tektronix 2215 A 60 MHz oscilloscope. Signal detection was accomplished using probes of the design presented in this paper. A typical setup for testing is shown in Figure-5.

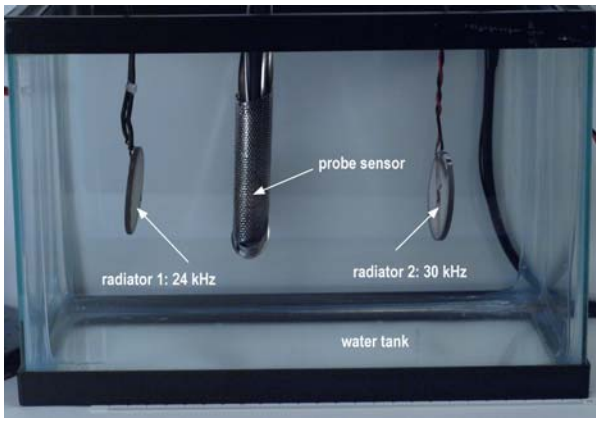

Figure-5. Test cell and setup for verifying probe performance.

Acoustic field model

A model approximation of the resulting wave form at the probe's sensor surface is computed from the one dimensional wave equation whose spatial and temporal amplitude, *y*, is given in equation 2 [20]:

$$y(x,t) = \sum_n \sum_i C_i \cos\left[\frac{2\pi}{\lambda_n}(ct - x_i) + \vartheta_i\right] \qquad (2)$$

The acoustic pressure amplitude at a location is the sum of the wave amplitudes arriving from the 24, 30 and 40 kHz components radiating from the transducers directly or by reflection, and accounted for by the index, *n*. Six rays were considered from each radiator: the direct ray from the face of the radiating transducer to the surface of the sensor along with reflected rays from the top, bottom, sides and back glass surfaces of the tank. The rays are counted by the index *i* in equation 2, and have an associated phase change given by φ_i in radians. λ_n are the wavelengths for each frequency component in meters, *c* is the acoustic velocity in water in meters per second, x_i are the ray path distances in meters and *t* is time in seconds. C_i are the relative amplitudes of each ray determined by the level of amplification of the driving voltages for the primary component, and by waveform analysis to size the induced coupling for the 40 kHz component. Unity reflection coefficients were used because the hard glass surface is purely reactive. Reflections from the far wall, and multiple reflections, are not included which are limitations in how well the model will fit the data.

RESULTS OF EXPERIMENTAL WORK

Predicted vs. measured signal

The response of a single shielded probe in a complex field produced by two radiators is recorded. With respect to the bottom left front corner of the test tank, the probe sensor is situated on a centerline 7 cm from the bottom of the test tank that lies between a disk radiator at 6.5 cm and second disk radiator at 21 cm for the first measurement. Then the second transmitter is moved from 21 to 24 cm for the second measurement. These measurements of field pressure, along with modeled pressure for the same configurations, are shown in Figure-6.

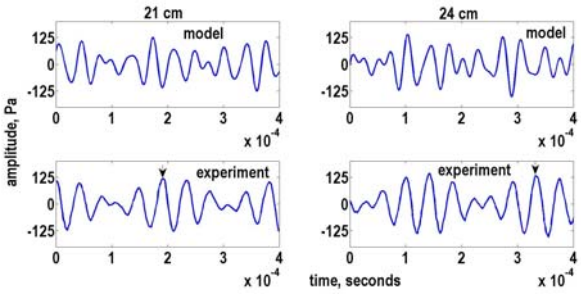

Figure-6. Measured acoustic field compared to modeled field with probe between two radiating transducers.

The radiator at 6.5 cm is broadcasting a continuous sine wave at 24 kHz along with a much smaller 40 kHz signal from transducer resonance coupling to the driving voltage. The radiator initially at 21 cm, then at 24 cm transmits a 30 kHz sine wave along with its induced 40 kHz component. The top row graphs of Figure-6 are the corresponding modeled acoustic signal obtained by first order ray tracing.

Shielded vs. unshielded probe measurements

Figure-7 shows how shielded and unshielded probe measurements were made in a complex acoustic environment allowing the EMR and acoustic signals to be identified. The radiating source transducer is driven by a 50 V_{pp}, 40 kHz, square wave on terminals A and B from a signal generator described in the apparatus section. A portion of two cycles of this driving signal as recorded by an oscilloscope connected to A and B are shown in the left callout of Figure-7. The radiating transducer smoothes the square wave slightly as it broadcasts an acoustic signal from surface vibration caused by the piezoelectric effect into the water that follows direct and indirect (by reflections) paths to the probe sensor. Additionally, the voltage signal radiates EMR into the water since terminals A and B are submersed. This broadcasted acoustic signal is detected by the sensor of the probe from vibrations of its surface that are transformed into a voltage signal by the piezoelectric effect. If the Faraday cage is ungrounded, the electrodes plated on the probe's sensor surface pick up the EMR that becomes EMI when mixed in with the acoustic signal. The ungrounded and grounded voltage signal output from the probe on remote terminals C and D (the end of the grounded, shielded instrument cable attached to the probe) are shown in the right hand callouts. The signal strength of the ungrounded probe signal is of the order of 10 V_{pp}, while the real acoustic signal shown in the top right callout is only millivolts in magnitude. This same millivolt acoustic signal is seen in the lower right hand callout as a straight line with no detail.

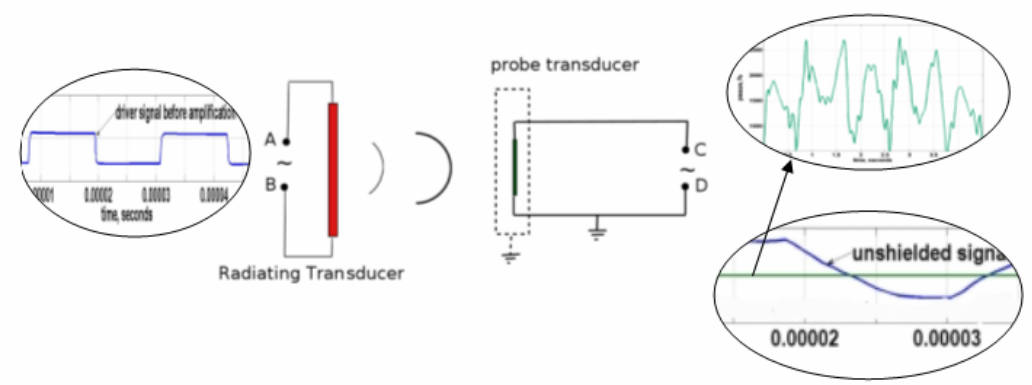

Figure-7. Transducer driving voltage signal impressed on the radiating transducer at terminals A and B (left callout), transformed by the response function of the radiator and broadcast into the water. Broadcasted signal, including reflections, is detected by the probe sensor housed in a Faraday cage, and transformed by the response function of the probe transducer. The resultant signal from the probe is output on terminals C and D which are attached to the oscilloscope.

The signal at the oscilloscope is shown in the callouts on the right, when cage is grounded (top), or ungrounded (bottom). The probe is 9 cm from the radiator. In both cases the negative lead of the probe transducer is grounded and incased in shielded instrument cable.

The response differences between grounding and ungrounding the insonated probe (shown in Figure-7 as a dotted rectangle around the probe sensor) can be further clarified by comparing the dominant frequency components contained in these waveforms which have been calculated using a Discrete Fourier Transform (DFT) obtained by numerical analysis solutions of:

$$X(k) = \sum_{j=1}^{N} x(j)\omega_N^{(j-1)(k-1)} \tag{3}$$

$$\omega_N = e^{\frac{(-2\ \pi\ i)}{N}}$$

where x is the vector of samples of the waveform, N is the sample frequency, k is the number of discrete sample points, and ω contains the sine and cosine frequency components contained in the sampled waveform. The computational result, X, is the vector of coefficients of the sine and cosine components contained in x. In the implementation of this solution the waveform sample vector is converted to equal increments, and a sampling frequency adequate for temporal resolution is selected. The calculated dominant frequencies for the signals shown in Figure-7 are plotted in Figure-8.

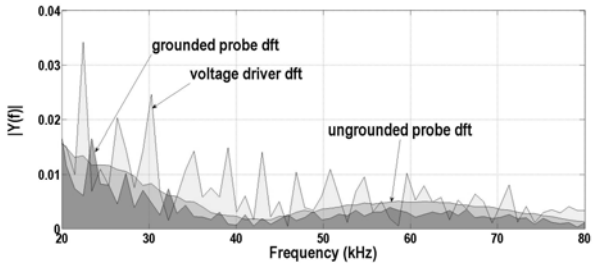

Figure-8. Discrete Fourier transform of normalized signals from (a) voltage impressed on the radiating transducer, labeled voltage driver dft, (b) signal from the grounded probe, labeled grounded probe dft, and (c) signal from the ungrounded probe, labeled ungrounded probe dft.

Phase as a function of position

The responses from two Faraday shielded probes having the design of Figure-1 are recorded when being insonified by a single transducer radiator for studying resolution and phase change. The positioning of the probes and the radiator are shown in Figure-9.

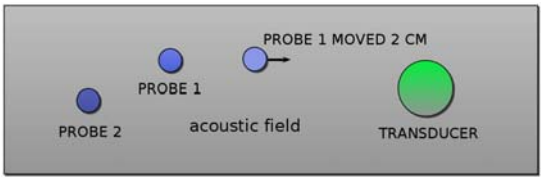

Figure-9. Schematic of experimental conditions (a) a radiating transducer insonifies two probes labeled 1 and 2; (b) probe 1 is then displaced in the horizontal direction by 2 cm moving closer to the source.

Figure-10 shows a comparison of the grounded probe response from the two probes in these two positions in the test tank when being insonified by the 5 cm disk radiator.

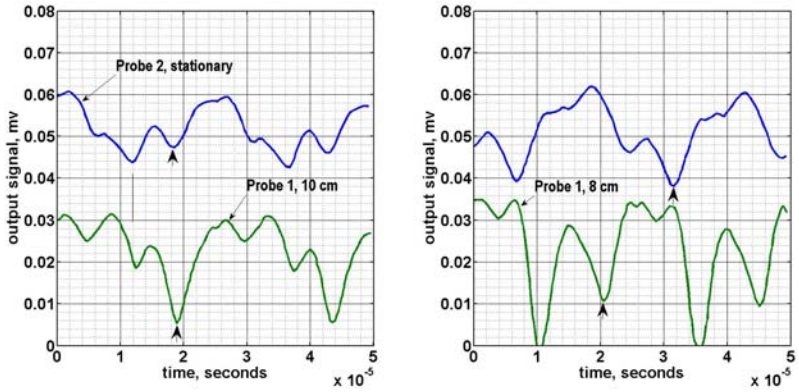

Figure-10. Grounded probe response for (a, left) probe distances of 10 and 14 cm from the source, and (b, right) probe distances of 8 and 14 cm from the source.

Two Lissajous plots were made using the grounded and ungrounded probe signals when separated by 6 cm, and are shown in Figure-11. These are made by connecting the signal from each probe to separate input channels of an oscilloscope set in the XY plotting mode and setting the gain of each channel to be the same.

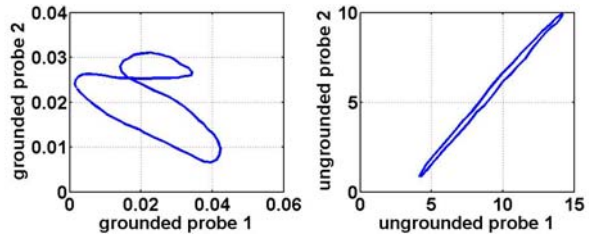

Figure-11. Lissajous plots for probe response when (a) grounded and (b) ungrounded for the probe positions in Figure-9 (b).

DISCUSSIONS

Predicted vs. measured signals

The correlation characterizing the fit of the predicted signal by ray tracing to the experimentally measured signal for the two opposing transmitter cases was determined from equation 4 [23] and plotted as a function of signal incremental displacement in Figure-12.

$$r_{xy} = \frac{\sum_{i=1}^{n}(x_i - \bar{x})(y_i - \bar{y})}{\sqrt{\sum_{i=1}^{n}(x_i - \bar{x})^2 \sum_{i=1}^{n}(y_i - \bar{y})^2}} \quad (4)$$

r is the correlation coefficient ranging from 0 for no relationship between curves x and y, and 1 when x completely matches y. n is the number of sample points, and the variables with the bar are the means of each distribution. The denominator is the equivalent of the product of the standard deviations of the two distributions. r^2 is a measure of the amount of variation in one curve that is related to the other curve. The maximum correlation obtained with lagging time between signals of 16.7 ms is 0.8. This is sufficient to assert that the measured waveform has its source in the radiated signature of the transducer and not from the driving voltage EMR because the measured signal correlates to the predicted signal from vibration of the face of the transducer established by transducer performance characteristics and not to the square wave impressed voltage constituting the EMR. Consequently, this probe design is capable of resolving high frequency components of a transmitted ultrasonic signal that are likely needed in determining energy input to sonochemistry mechanism models for ionization and polymerization as mentioned by Wu [1]. If much higher frequency components need to be resolved shrinking the physical PZT sensor may help. Alternatively a different PZT element with appropriate response range can be found. The movement of probe 1 closer to the source correctly shows a growth in measured signal amplitude. It can be seen in Figure-10 that the characteristics of the two curves change when probe 1 is moved, even though probe 2 remains in the same place. This is the result of the change in the complex acoustic field in the tank caused by a different reflection environment emanating from the structure of probe 1 when in its new position, and is further evidence of the probe's spatial sensitivity.

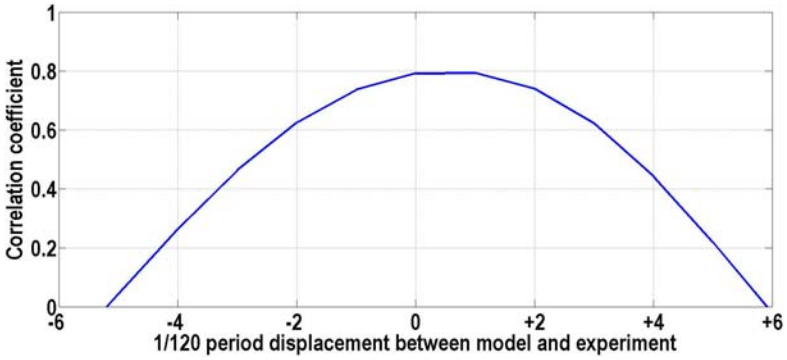

Figure-12. Correlation coefficient between the two waveforms in Figure-8 as a function of fractional period displacement between them.

Shielded vs. unshielded measurements

The grounded probe response in Figure-7 shown in the callout is approximately 150 millivolts peak to peak. By contrast, the ungrounded probe signal is more than 5000 millivolts peak to peak when driven by a 50 V peak-to-peak driving signal. Furthermore, the unshielded probe signal in Figure-7 is roughly the same square wave shape as the applied voltage to the transducer, and exhibits an integrated average phase which is constant because phase changes for the electromagnetic signal are too small to resolve.

Thus the grounded probe detects a complex acoustic signal that is .003 times smaller than the ungrounded signal generated by EMR.

The Discrete Fourier Transforms calculated for the 50 V_{pp} voltage driving signal, and the grounded and ungrounded probe signals reveal a series of sharp resonance peaks as expected from the Fourier series representing the spectrum of the square wave source. The normalized DFT of the ungrounded probe response shows the effect of processing the square wave voltage signal through both the radiating transducer and the probe's sensor while allowing the contribution from the dominant EMR emanating from the impressed high voltage driving signal. In doing this the ungrounded probe response removes the detail of the spectrum of the square wave broadcast signal from the radiating transducer thereby substantially removing acoustic field detail. By contrast, once the probe is grounded the detail of the broadcasted acoustic signal is restored as the peaks in the grounded DST demonstrate. Importantly, there is a difference in the spectrum of the broadcasted acoustic signal as measured by the grounded probe, and the spectrum of the square wave driving signal before it passes through the radiating transducer. This is apparent in the difference in the peaks not including the 2 peaks near 40 kHz where coincidence is expected.

Phase as a function of position

In interpreting Figure-11, it is known that Lissajous patterns on an oscilloscope will be inclined ovals, or circle patterns depending on the magnitude of the phase change for each major frequency component, while phase changes of only a few degrees will appear as an inclined straight line having a slope determined by the magnitude of the signals. The Lissajous patterns in Figure-11 confirm that a significant phase change occurs between grounded probes when one is displaced relative to the other, and the phase change vanishes upon ungrounding of the Faraday cage. Examination of plot 11 (a) reveals that the slope of the major oval has passed 90 degrees indicating a phase shift in excess of a quarter wavelength. It is also seen that the Lissajous pattern for (a) is in millivolts while in (b) it is about 10 Volts across.

The phase changes shown in Figures 10 and 11 can be understood as follows: when the probes are separated by a significant fraction of the radiated acoustic wavelength, and when both are grounded, phase change should be observed in comparing their output. If both are ungrounded, the signal being detected will be dominated by EMR from the transducer driving voltage, and little phase change should be observed. This is because the transmitted EMR is electromagnetic radiation traveling at the speed of light having a very short wavelength given by equation 5.

$$\lambda = c / f \tag{5}$$

where λ is the wavelength in meters, c is the velocity of light and f is the signal frequency in cycles per second. Thus the wavelength of the electromagnetic signal is much shorter than the acoustic signal. Since the transmitted pressure wavelength is 3.7 cm, a phase shift for an ~ 2 cm displacement would be near one half of a wavelength. Inspection of Figure-10 shows the phase shift of probe 1 which was moved approximately 2 cm closer to the source has a phase shift to an earlier time of about a half wave when comparable features of the two signals are examined (see arrows). The starting point of the curves will shift between Figures due to the triggering point of the oscilloscope.

CONCLUSIONS

A submersible ultrasonic acoustic pressure probe is presented and characterized which is designed for making pressure measurements in fluids near a strong

source of electromagnetic radiation. It is significantly isolated from electromagnetic signal contamination from the high voltage driving signal of the ultrasonic source because it employs shielding from a separately grounded Faraday cage. The efficacy of this shielding, and the sensitivity of the probe, is examined and proven by test cases. The first experiment shows that the probe can resolve the detail of a complex acoustic field according to theory; the second experiment demonstrates measurable difference in amplitude, frequency and phase from grounding compared to ungrounded designs, while the third experiment proves the probe is responding to the acoustic signal, not the EMR, by comparing phase changes.

An apparatus and method for calibrating the probe is developed and tested based on an instrumented force measuring beam which can be submersed into the same liquid environment. This beam is made from a copper strip onto which a narrow strain gauge is bonded, and having a pressure force target matching the probe's active element. Response of the beam to both gram weights, a static load, and to the dynamic load from the signal to be tested comprises a calibration method to produce a sub-standard from which the probe itself may be calibrated. Sub-standards may be created for each test frequency of interest.

It is seen that the probe is able to record waveform changes resulting from path differences on the order fractions of a wavelength. This can be useful in experiments in which the details of field exposure need to be resolved. Furthermore, the effective isolation of a probe by a grounded Faraday cage so as to better characterize an acoustic field level can be very important in determining dose from ultrasonic exposure. Without adequate isolation there is the possibility of overestimating ultrasonic dosage. Subsequent to this work, the author's laboratory has successfully miniaturized this design using a 5 mm active element encased in a metal connector shielded by screen wire to comprise the Faraday cage. The resulting small detector is suitable for insertion in small volumes where knowledge of pressure fields is important to understand system behavior. This probe design also has applications in small volume systems like sonochemical material manufacturing and protein degradation work in medical and food applications.

REFERENCES

[1] Wu C.I., *et al*. 2010. Ultrasound ionization of biomolecules. Rapid commun. mass sp. 24(17): 2569-2574.

[2] Edwards J., *et al*. 1976. Effect of ultrasonic cavitation on protein antigenicity. J. Acoust. Soc. Am. 59(6): 1513-1514.

[3] Marchioni C., *et al*. 2009. Structural changes induced in proteins by therapeutic ultrasounds. Ultrasonics. 49(6-7): 569-576.

[4] Gulseren I., *et al*. 2007. Structural and functional changes in ultrasonicated bovine serum albumin solutions. Ultrason. Sonochem. 14(2): 173-183.

[5] Suslick K., *et al*. 1994. Characterization of sonochemically prepared proteinaceous microspheres. Ultrason. Sonochem. 1(1): s65-s68.

[6] Gedanken A. 2004. Using sonochemistry for the fabrication of nanomaterials. Ultrason. Sonochem. 11 (12) : 47-55.

[7] Aurbach D. 2002. Nanoparticles of SnO Produced by Sonochemistry as Anode Materials for Rechargeable Lithium Batteries. Chem. Mater. 14(10): 4155-4163.

[8] Shariat-Panahi S. *et al*. 2009. Design and test of a high-resolution acquisition system for marine seismology. IEEE Instrumentation and Measurement Magazine. 12(I2): 8-15.

[9] Felizardo M. *et al*. 2008. Improved acoustic instrumentation of the SIMPLE detector. Nucl Instrum Methods. 585: 61-68.

[10] Soudagar S.R. and Samant S.D. 1995. Semiquantitative characterization of ultrasonic cleaner using a novel pressure intensity probe. Ultrason. Sonochem. 2(1): s49-s52.

[11] Bushberg J., *et al*. 2002. The Essential Physics of Medical Imaging. 2nd Ed., Lippencott Williams and Wilkins, Philadelphia, PA. p. 484.

[12] Martin C J and Law A N R. 1983. Design of thermistor probes for measurement of ultrasound intensity distributions. Ultrasonics. 21(I2): 85-90.

[13] Pugin B. 1987. Qualitative characterization of ultrasound reactors for heterogeneous sonochemistry. Ultrasonics. 25(1): 49-54.

[14] Durkee J. 2006. Management of Industrial Cleaning Technology and Processes. 1st Ed, Elsevier. p. 368.

[15] Witte R.S. et al. 2008. Inexpensive acoustoelectric hydrophone for mapping high intensity ultrasonic fields. J. Appl. Phys. 104, p. 054701 1-3.

[16] Morse P.M., Ingard K.U. 1968. Theoretical Acoustics. McGraw-Hill Book Company; New York, USA. p. 381, p. 269.

[17] Lewin P.A. 2000. Sensitivity of ultrasonic hydrophone probes below 1 MHz. Ultrasonics. 38: 135-139.

[18] 1996. Ultrasonic Power Output Measurement by Pulsed Radiation Pressure. J. Res. Natl. Inst. Stan. 101(5): 659-669.

[19] Ziskin M.C. and Lewin P.A. 1993. Ultrasonic Exposimetry, CRC Press. p. 133.

[20] Beranek Leo. 1971. Noise and Vibration Control. McGraw-Hill Book Company. p. 15.

[21] Chen H. *et al*. 2011. Blood Vessel Deformations on Microsecond Time Scales by Ultrasonic Cavitation. phys rev lett. 106, 034301, p. 106.

[22] Miki Y. 1990. Acoustical properties of porous materials-Modifications of Delany-Bazley models, J. Acoust. Soc. Jpn. p. 21, (E) 11, 1.

[23] Fisher R.A. 1936. Statistical Methods for Research Workers. 6th Ed. Oliver and Boyd, Edinburgh. p. 185.